- Technical Paper -

FIBER-BASED ANALYSIS OF REINFORCED CONCRETE WALLS WITH END REGION CONFINEMENT: SENSITIVITY TO MODELING CHOICES

Emine KOSE[*1], Naresh SUBEDI[*2], Susumu KONO[*3], David MUKAI[*4]

ABSTRACT

A number of stress-strain relationships for concrete and expressions to calculate the plastic hinge length (l_{ph}) have been suggested for fiber-based analysis of RC walls. However, no consensus exists regarding the appropriate modeling combination to accurately reproduce the flexural response. Three reinforced concrete walls with different end confinements were numerically modeled to study the effects of stress-strain relation of concrete and the equivalent plastic hinge length on the load-drift relations. Best combinations of stress-strain relationship (for concrete) and l_{ph} are identified for the walls considered.

Keywords: concrete confinement, fiber model, response sensitivity, plastic hinge length, stress-strain relationship

1. INTRODUCTION

Reinforced concrete (RC) walls are one of the most commonly used structural systems for mid- and high-rise buildings. Despite their widespread use, RC walls suffered severe damage in recent earthquakes, such as the 2010 Maule (Chile) Earthquake and the 2011 Christchurch (New Zealand) Earthquake, some even leading to the collapse of the building [1]. Reconnaissance studies following the earthquakes have reported that the damages were primarily caused by insufficient confinement and detailing in the end regions. These observations have highlighted the need for proper detailing of RC walls to improve the deformation capacity under seismic load. Following these events, a number of experimental and analytical studies have been conducted to develop guidelines for end region confinement of RC walls [1-3].

In the last two decades, several numerical modeling approaches have been developed to simulate the flexural response of RC walls [4-6]. Among them, the fiber-based modeling approach, in which the wall cross-section is discretized into fibers and the fiber response is defined by uniaxial stress-strain relationships of concrete and reinforcement, balances the accuracy and computational efficiency for design applications. The accuracy of the fiber-based model is primarily controlled by the stress-strain relationships used for the concrete. A number of stress-strain relationships and empirical expressions have been proposed to characterize the response of unconfined and confined concrete in RC members [7-10]. However, there is no consensus regarding the appropriate stress-strain relationship for simulating the flexural response of RC walls. A comparative study evaluating the influence of different stress-strain models of concrete on the global (load-deformation) response of walls is still lacking.

Beam-column elements with distributed-plasticity formulation produce non-objective (or mesh-sensitive) responses when used to simulate the softening response of structural components [11, 12]. Modified integration methods have been proposed as a workaround for this mesh sensitivity issue, where the integration weight of the most-strained integration point is scaled to match the equivalent plastic hinge length, l_{ph} [12]. This workaround necessitates an appropriate value of the predefined length l_{ph}. Although several empirical expressions have been proposed to obtain the l_{ph} of RC walls, the existing expressions produce different values of l_{ph}. The appropriate l_{ph} for RC walls is still a topic of debate among researchers, and the choice of one value over the other is highly subjective. A study comparing the global response obtained using different expressions for l_{ph} can shed light on the expected range of responses from the fiber-based analysis.

The present study addresses the issues highlighted in the previous paragraphs by comparing the load-deformation response obtained using different combinations of concrete stress-strain relationship and l_{ph}. The simulated responses are compared with the experimental results of three RC walls with different end confinement tested in the author's research group. The best combination of the stress-strain relationship and l_{ph} for the selected walls is identified. The results presented will help to make appropriate modeling choices for the design and analysis of RC walls.

2. TEST SPECIMEN PROPERTIES

Three specimens (MC, SC, HN) tested under

*1 PhD Student, Dept. of Architecture and Building Eng., Tokyo Institute of Technology, JCI Student Member
*2 Postdoctoral Researcher, Laboratory for Materials and Structures, Tokyo Institute of Technology
*3 Professor, Institute of Innovative Research, Tokyo Institute of Technology, JCI Member
*4 Associate Professor, University of Wyoming and Visiting Professor, Tokyo Institute of Technology

Table 1 Properties of wall specimens

Specimen	h_w/l_w	Shear span	Confined end region			Wall panel		Axial load (axial load ratio)
			A_{ch} (mm^2)	Long. rebar	Shear rebar	Thickness (mm)	Vertical and Horizontal rebars	
MC	0.97 (1700/1750)	1.37 (loading point = 2400 mm)	120×250 (84×214)	10-D10 (2.56%)	4-D4@80 (1.36%)	120	2-D4@50 (0.47%)	600 kN (0.1)
SC			120×150 (84×114)	6-D10 (2.70%)	2-D4@40 (1.46%)			
HN			120×450 (84×414)	10-D10 (1.38%)	4-D4@40 (2.61%)			1200 kN (0.2)

h_w/l_w: aspect ratio, h_w: wall hight, l_w: wall length, A_{ch}: the area of confined end region (values in parentheses are the confined region dimensions measured between stirrups centerlines), percentages correspond reinforcement area ratios.

reverse cyclic loading with different end region confinements were selected for this study [13]. These walls (40%-scale specimens) have the same shear span ratio (1.37) and two different axial load levels ($0.1A_g f'_c$ and $0.2A_g f'_c$). Here A_g is gross cross-section area and f'_c is compressive strength of concrete. Reinforcement details and mechanical properties of concrete and reinforcement of the wall specimens are summarized in Table 1 and Table 2, respectively. For more details of the experimental results and observations please refer to reference [13].

All three specimens have the same height, length, and wall thickness, but they have different confined areas in the end regions. Figure 1 shows the reinforcement details of the walls. The crack pattern of the walls at the peak load is shown in Fig. 2. All three specimens exhibited a flexure-controlled response.

Table 2 Mechanical properties of concrete and reinforcement

Concrete properties			
Specimen	Compressive Strength (MPa)	Young's Modulus (GPa)	Splitting Tensile Strength (MPa)
MC	29.6	33.0	2.60
SC	27.5	29.5	2.24
HN	27.8	31.0	2.52
Steel properties			
Reinforcing Bar	Yield Strength (MPa)	Young's Modulus (GPa)	Ultimate Strength (MPa)
D4	395	190	524
D10	385	196	524

3. NUMERICAL MODEL

Fig. 3(a) shows the schematic of fiber-based model used in the present study. A force-based beam-column element with six integration points is used to model the wall. The modified Gauss-Radau integration scheme [12] was used to scale the integration weight of the bottommost integration point to match the specified plastic hinge length, l_{ph}. Elastic shear deformation and flexural deformation were considered in numerical model, but the effect of pull out of longitudinal reinforcement was neglected. All analyses were conducted using the open-source computational framework *OpenSees*.

3.1 Stress-strain relationship of concrete

The wall cross-section was discretized into unconfined and confined concrete regions, as shown in Fig. 3(b). For the unconfined concrete, the stress-strain relationships of Kent-Park [7] and Mander [8] were

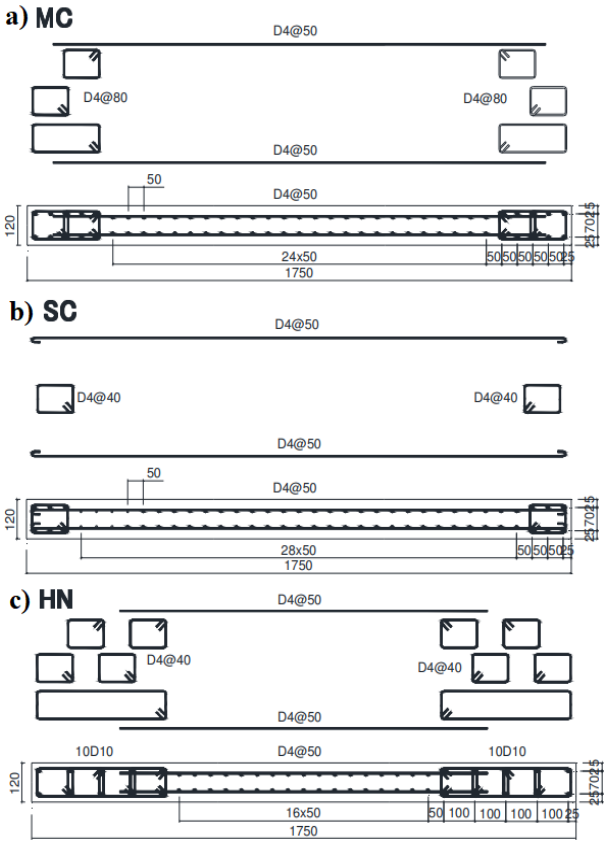

Fig. 1 Reinforcement details of the specimens

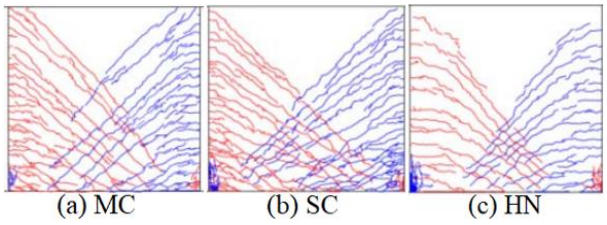

Fig. 2 Crack pattern at peak load (schematic for lower-half of the specimens)

considered for evaluation (Fig. 4(a)). In the Kent-Park model, concrete's residual stress is retained even after it reaches the ultimate strain. In contrast, the Mander model completely disregards the contribution of concrete once it reaches the ultimate strain, mimicking the spalling of cover concrete.

For confined concrete, four commonly used models to obtain the stress-strain relationships of RC members (viz., Kent-Park [7], Mander [8], Sheikh [9], and Saatcioglu [10]) were selected. Fig 4(b) compares the stress-strain relationship obtained according to the four approaches for specimen HN. Confined concrete strength is calculated with the equation $f'_{cc} = 0.85K_s f'_c$ in Sheikh model. Here, f'_c is compressive strength of concrete and f'_{cc} is confined concrete strength. The model uses a reduction factor of 0.85 for the concrete compressive strength. Also, a parameter K_s is used to calculate the concrete strength gain due to linear lateral reinforcement. For specimen HN, the strength enhancement factor K_s was approximately 1. Thus, confined concrete strength did not increase, on the contrary, a 15% decrease was observed in the strength since it was multiplied by 0.85. It is observed that the Sheikh model yields the lowest confined concrete strength, whereas the Saatcioglu model generally yields larger concrete strength compared to the other models. Regarding the post-peak response, Mander model tends to have more gradual strength-degradation, whereas the Saatcioglu model gives steeper degradation. These differences are expected to influence the lateral load-deformation response obtained from the analysis. The hysteretic behavior of each concrete model was based on the loading-unloading rules developed by Yassin [15].

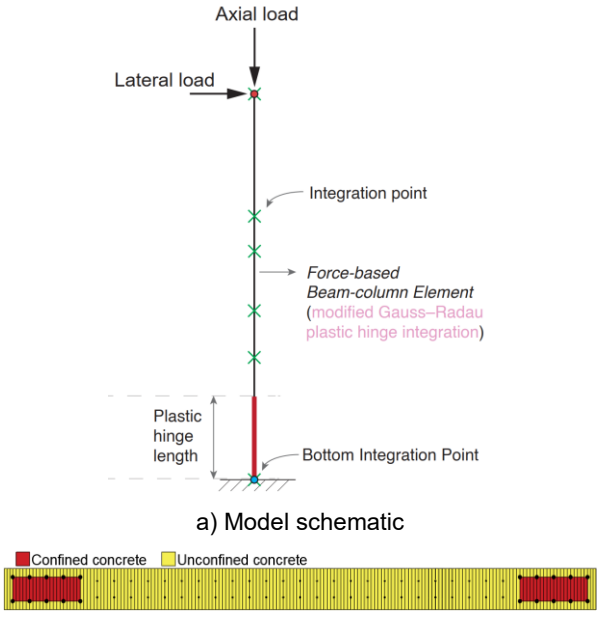

a) Model schematic

b) Section discretization

Fig. 3 Details of the numerical model

3.2 Stress-strain relationship of reinforcement

A bilinear stress-strain relationship with post-yield hardening ratio of 0.05 was used for the longitudinal reinforcement. Hysteretic behavior of the reinforcement was defined according to the Menegotto-Pinto rules.

3.3 Plastic hinge length

Numerous empirical expressions are available to calculate plastic hinge length of RC walls [14]. The five most commonly used expressions for l_{ph} are summarized in Table 3 [16-20] for discussion. Here, L_w is wall length, k is a parameter to reflect the spread of plasticity, H_e is effective height of the wall, d_{bl} is the diameter of the longitudinal reinforcement, f_{ye} is the expected yield strength of reinforcement ($f_{ye}=1.1f_y$), $f'c$ is compressive strength of the concrete, ALR is axial load ratio, and ρ_{sh} is the transverse reinforcement ratio.

Among the five expressions considered, two (Bohl-Adebar and Kazaz) consider the effect of axial load ratio on l_{ph}. The ASCE 41-06 equation does not consider the

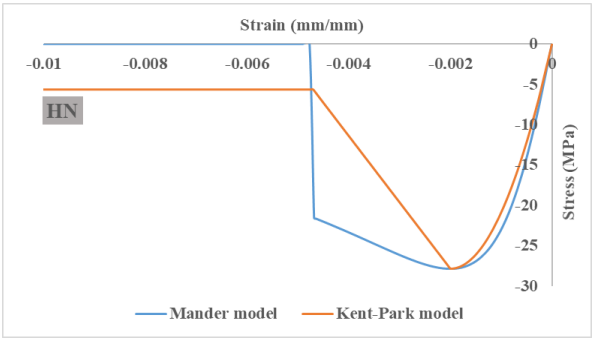

a) Unconfined concrete

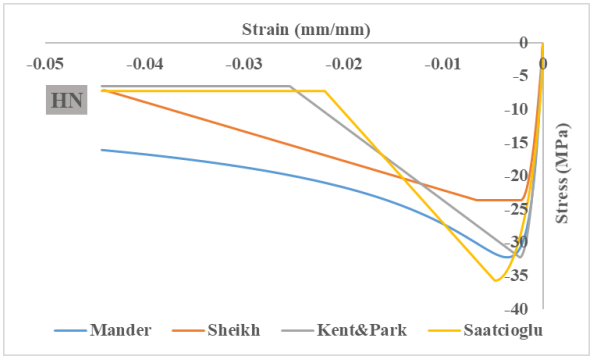

b) Confined concrete

Fig. 4 Stress-strain relationships for concrete

Table 3 Descriptions of l_{ph} models
(calculated l_{ph} are in mm)

Recommendations	Expressions of plastic hinge length	MC	SC	HN
ASCE/SEI 41-06	$l_{ph} = 0.5L_w$	875	875	875
Paulay&Priestley	$l_{ph} = kH_e + 0.2L_w + 0.022f_{ye}d_{bl}$	642	642	642
Eurocode 8	$l_{ph} = {}^{H_e}/_{30} + 0.2L_w + 0.11\left({}^{d_{bl}f_y}/_{\sqrt{f'_c}}\right)$	530	533	532
Bohl&Adebar	$l_{ph} = (0.2L_w + 0.05H_e)(1 - 1.5ALR) \le 0.8L_w$	425	425	350
Kazaz	$l_{ph} = 0.27L_w(1 - ALR)\left(1 - {}^{f_y\rho_{sh}}/_{f'_c}\right)\left({}^{H_e}/_{L_w}\right)^{0.45}$	499	441	404

effect of wall height on l_{ph}. Only Kazaz's equation considers the transverse reinforcement ratio in the l_{ph} calculation. The ASCE 41-06 gives the largest l_{ph} (875 mm) and the Bohl-Adebar equation gives the smallest l_{ph} (425 mm for SC and MC, 350 mm for HN) for the three specimens considered.

4. ANALYSIS RESULTS AND DISCUSSION

4.1 Effect of unconfined concrete model

Figure 5 shows the comparison of the shear force-drift (Q-R) response obtained using the two unconfined concrete models. Results for specimen SC (which has the smallest confined region; ref. Table 1) are presented because this specimen has the largest unconfined concrete area. This model used the Kent-Park relationship for the confined concrete (other stress-strain relationships were very similar except for the Sheikh model) and l_{ph} according to Eurocode-8 (as an intermediate value).

It is observed from Fig. 5 that the unconfined concrete models influenced the peak shear force and initiation of the strength degradation in the analysis (around 0.7% drift). Mander model produced a larger capacity due to more gradual strength degradation in the stress-strain relationship compared to the Kent-Park model (see Fig. 4(a)). However, the Q-R curve exhibited more abrupt strength-degradation once the unconfined concrete reached ultimate strain. This observation is attributed to the fact that the unconfined concrete fibers completely lose the capacity in the Mander model, whereas they retain some residual strength (20% of the

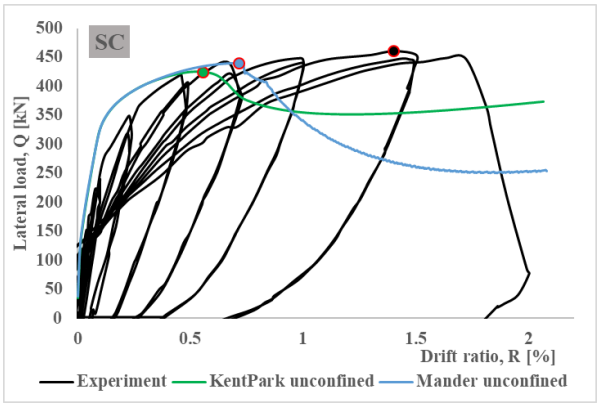

Fig. 5 Effect of unconfined concrete model on shear force-drift response of specimen SC.

compressive strength) in the Kent-Park model. These effects are less pronounced for the other two specimens (MC and HN) because of the relatively smaller area of the unconfined concrete. Furthermore, the influence of unconfined concrete model is more evident for models with smaller l_{ph} (Bohl-Adebar and Kazaz) as the ultimate strain limit is reached at a smaller drift. The Kent-Park unconfined concrete model is used for all analyses presented in the subsequent sections.

4.2 Effect of confined concrete model

Figure 6 compares the shear force-drift response obtained using the four confined concrete models for specimen HN. This specimen has the largest confined region (ref. Table 1); therefore, the simulated response is expected to be more sensitive to the choice of the confined concrete model. The results presented in Fig. 6 used l_{ph} according to Eurocode-8 (as an intermediate value).

Analysis results in Fig. 6 are directly correlated with the nature of the stress-strain relationships of confined concrete shown in Fig. 4(b). The Sheikh model (with the lowest confined concrete strength) yields a smaller capacity, and the Saatcioglu model (with the highest confined concrete strength) yields the largest capacity. The Saatcioglu model and Mander model produce similar overall monotonic responses. However, the Mander model results in a more abrupt reduction in capacity once the ultimate strain is reached around 1.4% drift. All four models underestimated the envelope curve obtained from the experiment.

For the other two specimens (MC and SC), similar responses are obtained using different confined concrete models except for the Sheikh model, which consistently produces lower strengths.

4.3 Effect of plastic hinge length

Analysis results obtained using different plastic hinge lengths (ref. Table 3) are compared in Fig. 7 for specimen HN. Confined concrete model of Mander was used in the analysis. The plastic hinge length obtained according to ASCE 41-06 was not considered, as the value was unreasonably large ($l_{ph} > 0.5H_w$) for all specimens.

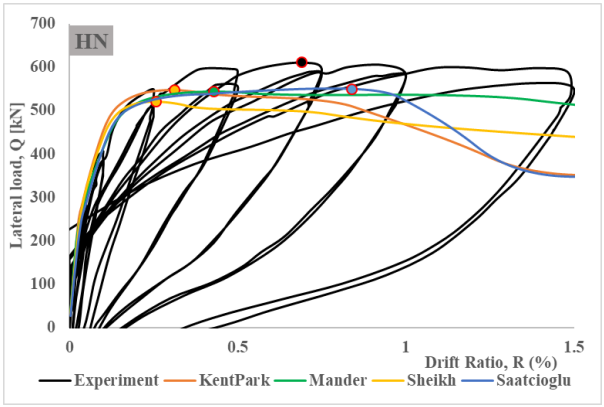

Fig. 6 Effect of confined concrete model on shear force-drift response of specimen HN.

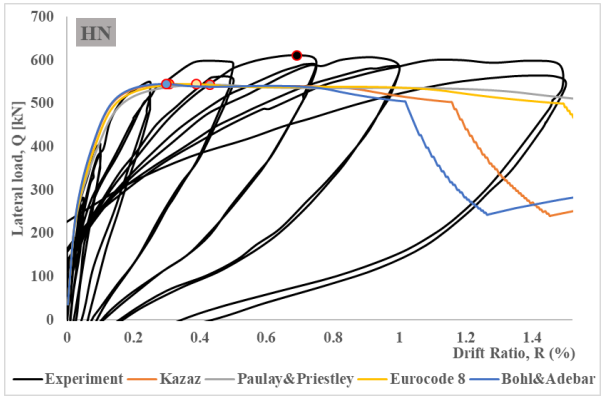

Fig. 7 Effect of different plastic hinge lengths on shear force-drift response of specimen HN.

Figure 7 shows that the plastic hinge length (l_{ph}) has a negligible effect on the peak strength but controls the drift corresponding to the initiation of strength

degradation (or, equivalently, the ultimate drift capacity). A smaller value of l_{ph} results in earlier strength degradation because larger strains are developed, and the strain reaches in the post-peak region of the stress-strain relationship at a smaller drift compared to a model with a larger l_{ph}. Accordingly, a small l_{ph} (e.g., Bohl-Adebar and Kazaz) can underestimate the drift capacity and vice-versa. Similar results were obtained for the other two specimens (MC and SC).

For the specimens considered, l_{ph} calculated according to Eurocode-8 and Paulay & Priestley equations reasonably simulated the envelope response obtained from the experiment. The equations proposed by Bohl & Adebar, and Kazaz resulted in earlier strength degradation than that observed in the experiment.

4.4 Cyclic response

The combinations of stress-strain models and l_{ph} identified to simulate the envelope response of the three RC wall reasonably are used in this section to simulate the cyclic response. The best combinations of concrete model and l_{ph} was determined based on comparison of peak shear force, residual drift, and overall energy dissipation, with the experimental results. The following model combinations were found to consistently produce good results for the three specimens: confined concrete models of Mander or Saatcioglu with the l_{ph} calculated according to Eurocode-8 or Paulay & Priestley. The Kent-Park model was used for the unconfined concrete in all analyses. As an example, Figure 8 shows the results obtained using one suggested combination using the Mander confined concrete model and plastic hinge length according to Paulay & Priestley. It is observed that this combination reasonably simulated the overall cyclic response, including the residual drift and the loading-unloading response. However, all considered approaches slightly underestimated the envelope response of the three specimens, especially for specimen HN in the positive loading cycle. Specimen HN had the largest confined area and dense shear reinforcement (ref. Table 1). One possible reason for the underestimation could be that the calculated confined concrete strength and ductility enhancement was smaller compared to the actual value. More experimental studies on highly-confined RC walls are needed to verify this proposition.

For design applications in which deformation capacity of RC walls is required, the drift corresponding to the limit compressive strain obtained from Eq. (1), proposed by Mander [8], can be taken as the ultimate drift capacity.

$$\varepsilon_{cu} = 0.004 + \frac{1.4\rho_s f_{yh}\varepsilon_{sm}}{f'_{cc}} \qquad (1)$$

In Eq. (1), ρ_s is the volumetric ratio of transverse reinforcement in confined end regions, f_{yh} is the yield strength of confining reinforcement, ε_{sm} is the limit strain of confining reinforcement (a value of 0.005 yields good agreement with the experimental results [13]) and f'_{cc} is the confined concrete compressive strength.

5. CONCLUSIONS

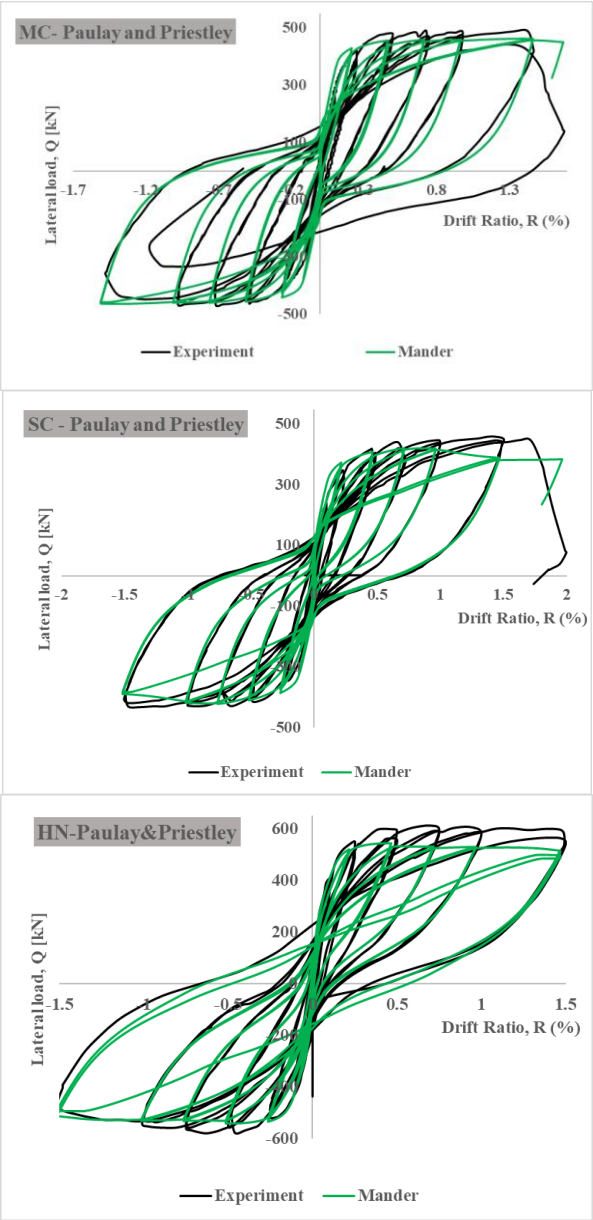

Fig. 8: Cyclic response of the specimens obtained from analysis and experiment.

The following conclusions are drawn based on the results and discussion presented in this study.

(1) Stress-strain relationship of unconfined concrete affects the peak strength and the drift at the initiation of strength degradation for RC walls with relatively small confined end regions. These effects were less pronounced for walls with larger confined end regions.

(2) The Sheikh model consistently gave lower confined concrete strength and ductility enhancement among the four confined concrete models. As a result, this model considerably underestimated the shear force-drift response obtained from the experiment, especially for the specimen with larger confined end regions.

(3) A smaller plastic-hinge length (l_{ph}) results in higher strains in the wall cross-section and, consequently,

earlier strength-degradation in the shear force-drift response. The ultimate drift capacity obtained from the analysis is very sensitive to the l_{ph} used in the numerical model.

(4) For the RC walls considered, the combination of the Mander confined concrete model, Kent-Park unconfined concrete model, and plastic-hinge length (l_{ph}) according to Paulay & Priestley yielded good agreement with the experimental results. Similar results were obtained using Saatcioglu confined concrete model and l_{ph} according to Eurocode-8.

Future studies should verify these findings with the test data covering a more comprehensive range of wall geometries, material properties, and axial load ratios.

ACKNOWLEDGEMENT

The first author would like to express her gratitude to the Turkish Government for the financial support for her Doctoral studies. The authors are also thankful to the WRH program (International Research Frontier Initiative), and Collaborative Research Project (MSL) at the Tokyo Institute of Technology and Dr. M. Tani (Kyoto Univ.) for their generous support of this research.

REFERENCES

[1] Taleb, R., Watanabe, H., & Kono, S. (2018). Numerical study on the ultimate deformation of RC structural walls with confined boundary regions. *Periodica Polytechnica Civil Engineering*, *62*(1), 191-199.

[2] Segura Jr, C. L., & Wallace, J. W. (2018). Impact of geometry and detailing on drift capacity of slender walls. *ACI Structural Journal*, *115*(3), 885-895.

[3] Kim, S. H., Lee, E. K., Kang, S. M., Park, H. G., & Park, J. H. (2021). Effect of boundary confinement on ductility of RC walls. *Engineering Structures*, *230*, 111695.

[4] Kolozvari, K., Arteta, C., Fischinger, M., Gavridou, S., Hube, M., Isakovic, T., ... & Wallace, J. (2018). Comparative Study of State-of-the-Art Macroscopic Models for Planar Reinforced Concrete Walls. *ACI Structural Journal*, *115*(6), 1637-1658.

[5] Kolozvari, K., Biscombe, L., Dashti, F., Dhakal, R. P., Gogus, A., Gullu, M. F., ... & Wallace, J. (2019). State-of-the-art in nonlinear finite element modeling of isolated planar reinforced concrete walls. *Engineering Structures*, *194*, 46-65.

[6] Pugh, J. S., Lowes, L. N., & Lehman, D. E. (2015). Nonlinear line-element modeling of flexural reinforced concrete walls. *Engineering Structures*, *104*, 174-192.

[7] Scott, B. D., Park, R., & Priestley, M. J. (1982). Stress-strain behavior of concrete confined by overlapping hoops at low and high strain rates. *ACI Journal Proceedings*, 79(1), 13–27.

[8] Mander, J. B., Priestley, M. J., & Park, R. (1988). Theoretical stress-strain model for confined concrete. *Journal of Structural Engineering (ASCE)*, *114*(8), 1804-1826.

[9] Sheikh, S. A., & Uzumeri, S. M. (1982). Analytical model for concrete confinement in tied columns. *Journal of the Structural Division (ASCE)*, *108*(12), 2703-2722.

[10] Saatcioglu, M., & Razvi, S. R. (1992). Strength and Ductility of Confined Concrete. *Journal of Structural Engineering (ASCE)*, *118*(6), 1590-1607.

[11] Calabrese, A., Almeida, J. P., & Pinho, R. (2010). Numerical issues in distributed inelasticity modeling of RC frame elements for seismic analysis. *Journal of Earthquake Engineering*, *14*(S1), 38-68.

[12] Scott, M. H., & Fenves, G. L. (2006). Plastic hinge integration methods for force-based beam–column elements. *Journal of Structural Engineering (ASCE)*, *132*(2), 244-252.

[13] Taleb, R., Kono, S., Tani, M., & Sakashita, M. (2014). Effects of end regions confinement on seismic performance of RC cantilever walls. In *Proceedings of the 10th US National Conference on Earthquake Engineering, Anchorage*, pp. 21-25.

[14] Hoult, R. (2022). Universal Plastic Hinge Length for Reinforced Concrete Walls. *ACI Structural Journal*, *119*(4), 75-83.

[15] Yassin, M. H. M. (1994). *Nonlinear analysis of prestressed concrete structures under monotonic and cyclic loads*. PhD dissertation, University of California, Berkeley.

[16] ASCE/SEI 41-06 (2007). *Seismic Rehabilitation of Existing Buildings*, American Society of Civil Engineers (ASCE): Reston, VA.

[17] Paulay, T., & Priestley, M. J. N. (1992) *Seismic Design of Reinforced Concrete and Masonry Buildings*, John Wiley & Sons, New York, 768 pp.

[18] EN 1998-3 (2005). *Eurocode 8: Design of Structures for Earthquake Resistance–Part 3: Assessment and Retrofitting of Buildings*, European Committee for Standardization, Brussels, Belgium.

[19] Bohl, A., & Adebar, P. (2011). Plastic Hinge Lengths in High-Rise Concrete Shear Walls. *ACI Structural Journal*, *108*(2), 148-157.

[20] Kazaz, İ. (2013). Analytical study on plastic hinge length of structural walls. *Journal of Structural Engineering (ASCE)*,*139*(11), 1938-195